Journal of Computational Physics 228 (2009) 2859–2873

Contents lists available at ScienceDirect

Journal of Computational Physics

journal homepage: www.elsevier.com/locate/jcp

A coupled arbitrary Lagrangian–Eulerian and Lagrangian method for computation of free surface flows with insoluble surfactants

Sashikumaar Ganesan [a,*], Lutz Tobiska [b]

[a] Department of Aeronautics, Imperial College of Science, Technology and Medicine, SW7 2AZ London, UK
[b] Institute of Analysis and Numerical Mathematics, Otto-von-Guericke University, PF 4120, D-39016 Magdeburg, Germany

ARTICLE INFO

Article history:
Received 27 February 2008
Received in revised form 3 November 2008
Accepted 23 December 2008
Available online 13 January 2009

Keywords:
Finite elements
ALE approach
Surfactant
Navier–Stokes equations

ABSTRACT

A finite element scheme to compute the dynamics of insoluble surfactant on a deforming free surface is presented. The free surface is tracked by the arbitrary Lagrangian–Eulerian (ALE) approach, whereas the surfactant concentration transport equation is approximated in a Lagrangian manner. Since boundary resolved moving meshes are used in the ALE approach, the surface tension, which may be a linear or nonlinear function of surfactant concentration (equation of state), and the Marangoni forces can be incorporated directly into the numerical scheme. Further, the Laplace–Beltrami operator technique, which reduces one order of differentiation associated with the curvature, is used to handle the curvature approximation. A number of 3D-axisymmetric computations are performed to validate the proposed numerical scheme. An excellent surfactant mass conservation without any additional mass correction scheme is obtained. The differences in using a linear and a nonlinear equation of state, respectively, on the flow dynamics of a freely oscillating droplet are demonstrated.

1. Introduction

Flows with surfactants are encountered in many industrial and biomedical applications such as enriched oil recovery, plastic production, detergents, drug delivery and lung mechanics. The presence of surfactant at the interface between two immiscible liquids reduces the surface tension. Therefore, a nonuniform distribution of surfactant generates variations in the surface tension which induce Marangoni convection. Further, adsorption and desorption of surfactants between the interface and the bulk phase may take place in the soluble surfactant case.

Apart from other challenges associated with computations of interfacial flows, the presence of surfactants makes the computation more challenging. The coupled time-dependent Navier–Stokes and surfactant transport equations have to be solved in a time-dependent domain, which is a priori unknown. Since the insoluble surfactant transport equation has to be solved on the moving interface, the interface has to be captured/tracked accurately. Therefore, the ability to study the precise effect of surfactants in fluid flows largely depends on the accuracy of the numerical scheme, which is used to solve the flow equations and the transport equation, simultaneously in a moving domain.

Interface capturing/tracking methods such as Volume-of-Fluid [16,18,27,29–31,40], Level set [17,26,32,35,36,42], Front Tracking [37,39], arbitrary Lagrangian–Eulerian [5,13,14,19,24,25] and pure Lagrangian [10,11] are popular approaches and often used in many numerical studies of clean, deforming interfacial flows. Each method has its own advantages and disadvantages. We note that the above literature list is not complete in the context of interfacial flow simulations. Methods

* Corresponding author.
E-mail addresses: s.ganesan@imperial.ac.uk (S. Ganesan), tobiska@mathematik.uni-magdeburg.de (L. Tobiska).
URLs: http://www3.imperial.ac.uk/people/s.ganesan (S. Ganesan), http://www-ian.math.uni-magdeburg.de/home/tobiska (L. Tobiska).

0021-9991/$ - see front matter © 2009 Elsevier Inc. All rights reserved.
doi:10.1016/j.jcp.2008.12.035

like immersed boundary element method and molecular dynamics simulation have also been used in computations of interfacial flows. Although, there have been many methods developed for capturing/tracking the interface in interfacial flows, numerical simulations incorporating the surfactant effects are rare. A Volume-of-Fluid based numerical scheme for computing interface flows with surfactants has been proposed in [30]. The formulation of the numerical scheme depends on the assumption of a linear equation of state, which relates the relation between the surface tension and the surfactant. Another numerical scheme based on the Volume-of-Fluid method has been developed for flows with insoluble surfactant in [20], in which an arbitrary equation of state could be used. Further, the authors have not determined the surfactant concentration directly, but by calculating the interfacial area and the surfactant mass, separately, the surfactant concentration obtained. A Level set based numerical scheme for two-dimensional interface flows with insoluble surfactant has been presented in [42]. In the context of Level set method, similar works on evolving quantities (but not necessarily surfactant concentration) along a moving interface can be found in [1,2]. A coupled Level set/Front Tracking has also been developed in [3] for studying the effects of the surfactants on capillary waves. In [28], an arbitrary Lagrangian–Eulerian (ALE) based finite element method has been developed for interfacial surfactant transport. The finite element discretisation used in [28] for the surfactant concentration differs from most of the existing mapped finite element codes, since the basis functions of the reference element varies cell-wise, i.e., each cell has a different finite element space but with same order and degrees of freedom. Further, to calculate the surface (tangential) gradient, a 3×3 system is solved at each quadrature point on the hypersurface.

In our numerical scheme, we use the ALE approach to track the moving interface, i.e., the interface is resolved by a moving mesh. Thus, the collection of edges/faces, which approximate the free surface, can be used at the same time as the computational domain for the transport equation. Further, the surface tension and local curvature can be included accurately. In our approach, we replace the curvature by the Laplace–Beltrami operator and apply integration by parts to reduce one order of differentiation associated with the curvature [6,7]. Thus, we end up with surface integrals with surface (tangential) gradient, which is similar as in the surfactant concentration transport equation.

The paper is organised as follows. In Section 2, the governing equations and their transformation into the dimensionless form are presented. Section 3 is devoted to the coupled ALE/Lagrangian finite element scheme used to approximate the solution of the flow equations and the surfactant concentration. Finally, in Section 4 computational results for validating the numerical scheme are presented.

2. Governing equations

2.1. Dimensional form of the flow equations

We consider a Newtonian incompressible fluid flow with insoluble surfactant which is bounded by a time-dependent domain $\Omega(t) \subset \mathbb{R}^d,\ d = 2, 3$. For simplicity, we assume that the entire boundary of $\Omega(t)$ is a free surface $\Gamma_F(t)$, i.e., $\Gamma_F(t) := \partial\Omega(t)$ and that gravitational effects can be neglected. In the time interval $(0, T]$, the fluid flow is described by the time-dependent incompressible Navier–Stokes equations

$$\rho\left(\frac{\partial u}{\partial t} + (u \cdot \nabla)u\right) = \nabla \cdot \mathbb{S}(u, p), \quad \nabla \cdot u = 0 \quad \text{in } \Omega(t). \tag{1}$$

Here, u is the velocity, p is the pressure, t is the time and ρ is the density. The stress tensor $\mathbb{S}(u, p)$ for the Newtonian incompressible liquid is given by

$$\mathbb{S}(u, p) = \mu\left(\frac{\partial u_i}{\partial x_j} + \frac{\partial u_j}{\partial x_i}\right) - p\delta_{i,j}, \quad i,\ j = 1, \ldots, d,$$

where μ is the dynamic viscosity, $(x_1, \ldots, x_d) \in \mathbb{R}^d$ and δ_{ij} is the Kronecker delta. At time $t = 0$ the domain and the velocity field are known:

$$\Omega(0) = \Omega_0, \quad u|_{t=0} = u_0.$$

On the free surface $\Gamma_F(t)$, we impose the kinematic condition

$$u \cdot \nu = w_f \cdot \nu$$

and the force balancing condition

$$\nu \cdot \mathbb{S}(u, p) \cdot \nu = \sigma(\Gamma)\mathcal{K}, \quad \tau_i \cdot \mathbb{S}(u, p) \cdot \nu = \tau_i \cdot \nabla\sigma(\Gamma)$$

for $i = 1, \ldots, d-1$ and any $t \in (0, T]$. Here, ν, and τ_i are the unit normal and tangential vectors, respectively, on the free surface $\Gamma_F(t)$. Further, w_f is the free surface velocity, $\mathcal{K}$ is the sum of the principal curvatures, Γ is the surfactant concentration and $\sigma(\Gamma)$ is the Γ dependent surface tension coefficient given by an equation of state (EOS). Often, see for example [9,28,43], a nonlinear Langmuir equation of state in the form

$$\sigma(\Gamma) = \sigma_0 + RT_a\Gamma_\infty \ln(1 - \Gamma/\Gamma_\infty), \tag{2}$$

is used. Here, σ_0 is the surface tension coefficient of the surfactant-free (clean) liquid, R is the ideal gas constant, T_a is the absolute temperature and Γ_∞ is the maximum surface packing surfactant concentration. When the variation of the surfactant concentration around a reference surfactant concentration Γ_1 is small, we can use the Henry's linear equation of state

$$\sigma(\Gamma) = \sigma_1 + RT_a(\Gamma_1 - \Gamma), \tag{3}$$

see for example [20,28]. Here, σ_1 corresponds to the surface tension in the reference phase.

2.2. Surfactant transport along a deforming free surface

2.2.1. Convection–diffusion equation for surfactant

The surfactant concentration along a deforming free surface is described by a scalar convection–diffusion equation with a source like term to account for the local changes in the free surface area. It reads:

$$\frac{\partial \Gamma}{\partial t} + \underline{\nabla} \cdot (\Gamma U) + \Gamma(u \cdot v)\underline{\nabla} \cdot v = D_s \underline{\Delta}\Gamma \quad \text{on } \Gamma_F(t), \tag{4}$$

see for e.g. [20,34,41]. Here, D_s is the surface diffusivity of the surfactant and $U = (u \cdot \tau_i)\tau_i = (u - (u \cdot v) \cdot v),\ i = 1, \ldots, d-1$, is the velocity along the free surface. The surface (tangential) gradient operator $\underline{\nabla}$ and the Laplace–Beltrami operator ($\underline{\Delta}$) are defined by

$$\underline{\nabla}\Gamma := \nabla\Gamma - (v \cdot \nabla\Gamma)v, \quad \underline{\Delta}\Gamma := \underline{\nabla} \cdot \underline{\nabla}\Gamma.$$

Note that in the definitions above we have assumed that Γ is defined not only on $\Gamma_F(t)$ but also in a certain neighbourhood. However, it is well-known that the restrictions of $\underline{\nabla}\Gamma$ and $\underline{\Delta}\Gamma$ on $\Gamma_F(t)$ depend only from values of Γ on $\Gamma_F(t)$. This has to be taken into account also in the boundary condition for the Navier–Stokes equation where

$$\tau_i \cdot \mathbb{S}(u,p) \cdot v = \tau_i \cdot \nabla\sigma(\Gamma) = \tau_i \cdot \underline{\nabla}\sigma(\Gamma).$$

We complete Eq. (4) by the initial condition

$$\Gamma|_{t=0} = \Gamma_0.$$

Note that no boundary condition has to be specified due to our assumption that the boundary $\Gamma_F(t)$ of $\Omega(t)$ is a closed surface.

2.2.2. Alternative form of the surfactant transport equation

In our numerical scheme, we use an alternative form of the surfactant concentration equation

$$\frac{\partial \Gamma}{\partial t} + U \cdot \underline{\nabla}\Gamma + \Gamma\underline{\nabla} \cdot u = D_s \underline{\Delta}\Gamma \quad \text{on } \Gamma_F(t), \tag{5}$$

see for example [8,23,43]. Here, the tangential divergence of the fluid velocity $\underline{\nabla} \cdot u$ is defined as the trace

$$\underline{\nabla} \cdot u = \mathrm{tr}((\mathbb{I} - v \otimes v)\nabla u).$$

Here, $\mathbb{I}$ and $\otimes$ denote the identity tensor and the vector direct product, respectively. We note that, when the free surface is not deforming, i.e., $u \cdot v = 0$, the standard form of the transport equation can be used. Further, the equivalence between Eqs. (4) and (5) can be shown by decomposing the velocity u in Eq. (5) by

$$\Gamma\underline{\nabla} \cdot u = \Gamma\underline{\nabla} \cdot ((u \cdot v)v) + \Gamma\underline{\nabla} \cdot U = \Gamma(u \cdot v)\underline{\nabla} \cdot v + \Gamma\underline{\nabla} \cdot U$$

and combining the last term and the term $U \cdot \underline{\nabla}\Gamma$ in Eq. (5).

2.3. Nondimensional form of the governing equations

To rewrite the Navier–Stokes equations (1) and the surfactant concentration equation (5) into a nondimensional form, we introduce the scaling factors L and U_{ref} as characteristic length and velocity, respectively. Further, we define the nondimensional variables as

$$\tilde{x} = \frac{x}{L}, \quad \tilde{u} = \frac{u}{U_{\mathrm{ref}}}, \quad \tilde{w} = \frac{w}{U_{\mathrm{ref}}}, \quad \tilde{t} = \frac{tU_{\mathrm{ref}}}{L}, \quad \tilde{p} = \frac{p}{\rho U_{\mathrm{ref}}^2}, \quad \tilde{\Gamma} = \frac{\Gamma}{\Gamma_\infty}.$$

In our model, with this scaling, the relevant dimensionless numbers (Reynolds, Weber and Peclet, respectively) are defined as

$$Re = \frac{\rho U_{\mathrm{ref}} L}{\mu}, \quad We = \frac{\rho U_{\mathrm{ref}}^2 L}{\sigma_0}, \quad Pe = \frac{U_{\mathrm{ref}} L}{D_s}.$$

Using these nondimensional parameters in the Navier–Stokes equations (1), and omitting the tilde afterwards, we obtain

$$\frac{\partial u}{\partial t} + (u \cdot \nabla)u = \nabla \cdot \mathbb{S}(u,p), \quad \nabla \cdot u = 0 \quad \text{in } \Omega(t) \tag{6}$$

with

$$\mathbb{S}(u,p) = \frac{1}{Re}\left(\frac{\partial u_i}{\partial x_j} + \frac{\partial u_j}{\partial x_i}\right) - p\delta_{ij}, \quad i,\ j = 1,\ldots,d.$$

Using the nonlinear equation of state (2), the nondimensional form of the force balancing condition becomes

$$\begin{aligned} v\cdot\mathbb{S}(u,p)\cdot v &= \frac{1}{We}(1 + E\ln(1-\Gamma))\mathscr{K}, \\ \tau_i\cdot\mathbb{S}(u,p)\cdot v &= -\frac{E}{We}\tau_i\cdot\left(\frac{\underline{\nabla}\Gamma}{1-\Gamma}\right), \end{aligned} \tag{7}$$

where E is the surfactant elasticity defined as $E = RT_a\Gamma_\infty/\sigma_0$. Similarly, using the linear equation of state (3), the nondimensional form of the force balancing condition becomes

$$\begin{aligned} v\cdot\mathbb{S}(u,p)\cdot v &= \frac{1}{We}\left(1 + E\left(\frac{\Gamma_1}{\Gamma_\infty} - \Gamma\right)\right)\mathscr{K}, \\ \tau_i\cdot\mathbb{S}(u,p)\cdot v &= -\frac{E}{We}\tau_i\cdot\underline{\nabla}\Gamma. \end{aligned} \tag{8}$$

Next, using these nondimensional variables in Eq. (5), and omitting the tilde afterwards, we obtain the nondimensional form of the surfactant concentration equation as

$$\frac{\partial\Gamma}{\partial t} + U\cdot\underline{\nabla}\Gamma + \Gamma\underline{\nabla}\cdot u = \frac{1}{Pe}\underline{\Delta}\Gamma \quad \text{in } \Gamma_F(t). \tag{9}$$

Remark 1. The surfactant concentration model described here can be directly extended to the case of non-closed free surfaces. Then, boundary conditions at $\partial\Gamma_{F_t}$ have to be added, for example inhomogeneous Dirichlet condition

$$\Gamma = \Gamma_g \quad \text{on } \partial\Gamma_{F_t}$$

or Neumann type boundary condition

$$\underline{\nabla}\Gamma\cdot n = \Gamma_N \quad \text{on } \partial\Gamma_{F_t},$$

where n denotes the intrinsic unit normal of $\partial\Gamma_{F_t}$ which is tangential to Γ_{F_t}, and Γ_g and Γ_N are given functions.

3. Numerical scheme

3.1. Coupled ALE-Lagrangian formulation

For solving the coupled problem (6) and (9) numerically, we need two meshes, one to decompose $\Omega(t)$ for the solution of the Navier–Stokes equation and one for decomposing the free surface $\Gamma_F(t) = \partial\Omega(t)$ and solving the surfactant concentration equation. The idea in this paper is to track the free surface by the arbitrary Lagrangian–Eulerian (ALE) approach and to use the discrete representation of $\Gamma_F(t)$ as a mesh to discretise Eq. (9). Indeed, to find the new shape of the domain Ω for the next time step, we solve Eqs. (6) and (9) with Γ given from the previous time step and move first the free surface with the fluid velocity u. Let $\Psi_{\Gamma_{F_t}}$ denote the resulting displacement of the free surface. Then, we compute the displacement (Ψ) of inner points of $\Omega(t)$ by solving the linear elasticity problem

$$\nabla\cdot\mathbb{T}(\Psi) = 0 \quad \text{in } \Omega(t), \quad \Psi = \Psi_{\Gamma_{F_t}} \quad \text{on } \Gamma_{F_t},$$

where $\mathbb{T}$ denotes the stress tensor given by

$$\mathbb{T}(\phi) = \lambda_1(\nabla\cdot\phi)\mathbb{I} + 2\lambda_2\mathbb{D}(\phi).$$

Here, $\mathbb{D}$ is the deformation tensor, λ_1 and λ_2 are the Lame constants, which are chosen to be $\lambda_1 = \lambda_2 = 1$ in our numerical tests. Once the displacement vector is calculated, we compute the mesh velocity w through the relation $w = d\Psi/dt$. After rewriting the Navier–Stokes equation (6) into the ALE form, it reads:

$$\frac{\partial u}{\partial t} + ((u-w)\cdot\nabla)u = \nabla\cdot\mathbb{S}(u,p), \quad \nabla\cdot u = 0 \quad \text{in } \Omega(t). \tag{10}$$

Note that we move the free surface with the liquid velocity, i.e., the surfactant concentration equation is considered in a Lagrangian manner. As a consequence, the Lagrangian form of Eq. (9) reads:

$$\frac{\partial\Gamma}{\partial t} + \Gamma\underline{\nabla}\cdot u = \frac{1}{Pe}\underline{\Delta}\Gamma \quad \text{in } \Gamma_F(t). \tag{11}$$

Due to the Lagrangian formulation, this transport equation does not contain any convection term. Thus, we do not need any stabilisation schemes while solving this transport equation by finite element methods.

3.2. The variational form

The solutions of the Navier–Stokes equations (10) and the surfactant concentration equation (11) are approximated by a finite element method. Thus, first we derive the variational form of the respective equations. To simplify the notation, from here on we use the subscript t to denote the time dependency, for example, Ω_t for $\Omega(t)$. Let $L^2(\Omega_t)$ and $H^m(\Omega_t)$, $m \geqslant 1$ be the usual Lebesgue and Sobolev spaces. We define $V = H^1(\Omega_t)^3$ and $Q = L^2(\Omega_t)$ as a velocity space and a pressure space, respectively, for Eq. (10). After incorporating the force balancing boundary condition, the variational form of Eq. (10) reads:

Given Ω_0 and $u(0)$, find $(u(t), p(t)) \in V \times Q$ such that for all $(v, q) \in V \times Q$

$$\left(\frac{\partial u}{\partial t}, \mathbf{v}\right) + a((u - w); u, v) - b(p, v) + b(q, u) = f(\mathscr{K}, v), \tag{12}$$

Here, $(\cdot, \cdot)$ denotes the inner product in $L^2(\Omega_t)$ and

$$a(\hat{u}; u, v) = \frac{2}{Re}\int_{\Omega_t} \mathbb{D}(u) : \mathbb{D}(v)\, dx + \int_{\Omega_t} (\hat{u} \cdot \nabla)u \cdot v\, dx$$

$$b(q, v) = \int_{\Omega_t} q \nabla \cdot v\, dx.$$

Further, for the nonlinear equation of state (7), $f(\mathscr{K}, v)$ is defined as

$$f(\mathscr{K}, v) = -\frac{1}{We}\int_{\Gamma_{F_t}} (1 + E\ln(1 - \Gamma))(v \cdot \nu)\mathscr{K}\, dS - \frac{E}{We}\int_{\Gamma_{F_t}} (v \cdot \tau_i)\left(\frac{\underline{\nabla}\Gamma}{1 - \Gamma}\right) \cdot \tau_i\, dS. \tag{13}$$

In case of the linear equation of state (8), we have

$$f(\mathscr{K}, v) = -\frac{1}{We}\int_{\Gamma_{F_t}} \left(1 + E\left(\frac{\Gamma_0}{\Gamma_\infty} - \Gamma\right)\right)(v \cdot \nu)\mathscr{K}\, dS - \frac{E}{We}\int_{\Gamma_{F_t}} (v \cdot \tau_i)\underline{\nabla}\Gamma \cdot \tau_i\, dS. \tag{14}$$

The curvature $\mathscr{K}$ in the surface integrals (13) and (14), respectively, is replaced by the Laplace–Beltrami operator $\underline{\Delta}$ of the identity id. More precisely, $\mathscr{K}\nu = -\underline{\Delta} id$, and integration by parts reduces one order of differentiation associated with the curvature. Hence, the surface integrals in (13) and (14) which contain the curvature, become

$$-\frac{1}{We}\int_{\Gamma_{F_t}} \underline{\nabla} id : \underline{\nabla}(v[1 + E\ln(1 - \Gamma)])dS = -\frac{1}{We}\int_{\Gamma_{F_t}} \underline{\nabla} id : \left([1 + E\ln(1 - \Gamma)]\underline{\nabla} v - \left[\frac{E}{1 - \Gamma}\underline{\nabla}\Gamma\right] \otimes v\right)dS$$

and

$$-\frac{1}{We}\int_{\Gamma_{F_t}} \underline{\nabla} id : \underline{\nabla}\left(v\left[1 + E\left(\frac{\Gamma_0}{\Gamma_\infty} - \Gamma\right)\right]\right)dS = -\frac{1}{We}\int_{\Gamma_{F_t}} \underline{\nabla} id : \left(\left[1 + E\left(\frac{\Gamma_0}{\Gamma_\infty} - \Gamma\right)\right]\underline{\nabla} v - E\underline{\nabla}\Gamma \otimes v\right)dS,$$

respectively. Next, to derive the variational form of Eq. (11), we set $W = H^1(\Gamma_{F_t})$. The variational form of Eq. (11) is obtained by multiplying it with a test function $\psi \in W$ and integration by parts for the diffusive term. It reads:

For a given free surface Γ_{F_t} and an initial distribution of surfactant concentration $\Gamma(0)$, find $\Gamma \in W$ such that for all $\psi \in W$

$$\left(\frac{\partial \Gamma}{\partial t}, \psi\right) + \frac{1}{Pe}(\underline{\nabla}\Gamma, \underline{\nabla}\psi) + (\Gamma\underline{\nabla} \cdot u, \psi) = 0. \tag{15}$$

Here, $(\cdot, \cdot)$ denote the inner product in $L^2(\Gamma_{F_t})$ and its vector-valued versions, respectively.

Finally, we mention that the three-dimensional variational formulation can naturally serve as a starting point for generating an axisymmetric variational form by transforming all integrals onto corresponding coordinates. For details we refer to Ganesan and Tobiska [14].

3.3. Calculation of the surface gradient

The calculation of the surface gradient can be done in two different ways. Either using the information from the surface mesh only, as in [28], or using the background mesh which is needed for the solution of the Navier–Stokes equation.

3.3.1. Method 1 (using the surface mesh)

Let K be a curved triangular/quadrilateral surface from the physical 3D space, and $\widehat{K}$ be their corresponding reference element in a parametric (ξ, η) plane. Then, we have the mapping $F_K : \widehat{K} \to K$ given by

$$x = x(\xi,\eta), \quad y = y(\xi,\eta), \quad z = z(\xi,\eta),$$

where $(\xi,\eta) \in \widehat{K}$. Further, let $\phi(x,y,z)$ be a function defined on K. Setting

$$\hat{\phi}(\xi,\eta) = \phi(x(\xi,\eta), y(\xi,\eta), z(\xi,\eta))$$

and applying the chain rule, we get

$$\frac{\partial\hat{\phi}}{\partial\xi} = \frac{\partial\phi}{\partial x}\frac{\partial x}{\partial\xi} + \frac{\partial\phi}{\partial y}\frac{\partial y}{\partial\xi} + \frac{\partial\phi}{\partial z}\frac{\partial z}{\partial\xi} = \nabla\phi\cdot\tau_1,$$
$$\frac{\partial\hat{\phi}}{\partial\eta} = \frac{\partial\phi}{\partial x}\frac{\partial x}{\partial\eta} + \frac{\partial\phi}{\partial y}\frac{\partial y}{\partial\eta} + \frac{\partial\phi}{\partial z}\frac{\partial z}{\partial\eta} = \nabla\phi\cdot\tau_2,$$

where $\tau_1 = \left(\frac{\partial x}{\partial\xi}, \frac{\partial y}{\partial\xi}, \frac{\partial z}{\partial\xi}\right)$ and $\tau_2 = \left(\frac{\partial x}{\partial\eta}, \frac{\partial y}{\partial\eta}, \frac{\partial z}{\partial\eta}\right)$ are tangential vectors on the surface. Then,

$$\nu = \frac{\tau_1\times\tau_2}{\|\tau_1\times\tau_2\|},$$

is the unit normal vector on the surface. Now, from

$$\underline{\nabla}\phi = \nabla\phi - (\nu\cdot\nabla\phi)\cdot\nu,$$

we have the following conditions

$$\underline{\nabla}\phi\cdot\tau_1 = \frac{\partial\hat{\phi}}{\partial\xi}, \quad \underline{\nabla}\phi\cdot\tau_2 = \frac{\partial\hat{\phi}}{\partial\eta}, \quad \underline{\nabla}\phi\cdot\nu = 0.$$

Thus, in case that only the function Φ on K, i.e., $\widehat{\Phi}$, is known, the surface gradient $\underline{\nabla}\Phi$ can be computed by solving the linear 3×3 system above.

3.3.2. Method 2 (using the background mesh)

Having in mind that the local finite element basis functions for solving the surfactant concentration equation are restrictions of local finite element basis functions with respect to a tetrahedral or a hexahedral mesh, the computation of the surface gradient is based directly on the formula

$$\underline{\nabla}\phi = \nabla\phi - (\nu\cdot\nabla\phi)\cdot\nu.$$

In all of our test examples, we will use this method to compute the surface gradient. This is possible since the two meshes in our coupled arbitrary Lagrangian–Eulerian and Lagrangian approach are closely related to each other.

4. Validation

The algorithm described above has been implemented in our in-house code MooNMD [21]. To validate the proposed numerical scheme, an array of computations for 3D-axisymmetric test cases are performed. Testing of the flow solver for the free surface flows in this numerical scheme has been reported in [12,14,15] and will not be discussed here. The considered test cases are the diffusion of surfactant over a static sphere, the convection of the free surface and the surfactant over an expanding sphere, the Marangoni convection over a sphere, and the freely oscillation droplet with and without surfactant.

In the first test case, we compare the numerical solution with the exact analytical solution of the surfactant concentration. In the second, the convection test case, the surfactant mass conservation is examined. The surfactant concentration profile and the influence of the Peclet number on the surfactant concentration profile are presented in the Marangoni test case. Finally, the shapes at different instance and the trajectories of some positions of a freely oscillating droplet with and without surfactant are presented.

In the computations, we always used isoparametric P_2 finite elements, i.e., continuous, mapped piecewise polynomials of second order for the spatial discretisation of the surfactant concentration. For the spatial discretisation of velocity and pressure in the Navier–Stokes equations, the inf–sup stable pair P_2^b, P_1^{disc} has been chosen, i.e., continuous, mapped piecewise polynomials of second order enriched with a cubic bubble function for velocity and discontinuous, mapped piecewise polynomials of first order for the pressure. Further, the fractional-step-ϑ scheme has been applied for the temporal discretisation, see e.g. [38]. The used surfactant elasticity and the reference surfactant concentration in all computations are $E = 0.2$ and $\Gamma_1 = 0.5$, respectively.

4.1. Diffusion test

We consider a fixed sphere of radius R and a nonuniform distribution of surfactant over the sphere. The surfactant will diffuse over the sphere and tends to become uniform when time goes to infinity. Taking into consideration that the Laplace–Beltrami operator on a sphere parametrised by spherical coordinates

$$x = R\cos\varphi\sin\theta, \quad y = R\sin\varphi\sin\theta, \quad z = R\cos\theta,$$

can be written in the form

$$\underline{\Delta}\Gamma = \frac{1}{R^2\sin\theta}\left\{\frac{\partial}{\partial\varphi}\left(\frac{1}{\sin\theta}\frac{\partial\Gamma}{\partial\varphi}\right) + \frac{\partial}{\partial\theta}\left(\sin\theta\frac{\partial\Gamma}{\partial\theta}\right)\right\},$$

we see that an exact analytical solution for the diffusion of a surfactant is given by

$$\Gamma(\theta,t) = 0.5 + 0.5\exp\left(\frac{-2t}{PeR^2}\right)\cos\theta, \quad 0 \leqslant \theta \leqslant \pi,$$

where θ is the angular coordinate measured from the pole of the sphere. This test example has been used earlier in [20]. We evaluated the errors in the surfactant concentration by using

$$L^\infty(L^2) := \sup_{(0,T)} \|\Gamma - \Gamma_h\|_{L^2(\Gamma_{F_t})}, \quad L^2(L^2) := \left(\int_0^T \|\Gamma - \Gamma_h\|^2_{L^2(\Gamma_{F_t})}\right)^{\frac{1}{2}},$$

where

$$\|\Gamma - \Gamma_h\|_{L^2(\Gamma_{F_t})} = \left(\int_{\Gamma_F(t)} (\Gamma - \Gamma_h)^2\right)^{\frac{1}{2}}.$$

The coarse mesh (Level 1) contains 101 degrees of freedom for the surfactant concentration. The finer mesh levels (Level 2–4) are obtained by successively refining the initial coarse mesh uniformly. The computed errors for $Pe = 1$ in the L^∞- and the L^2-norm for an unit sphere at time $T = 2$ are presented in Fig. 1. In this computation, a linear equation of state with $\Gamma_\infty = 1$ has been used. Even on the coarse mesh, the error is very small. We observe a convergence order of about 3.9.

4.2. Convection test

One important property that reflects the accuracy of a numerical scheme is the mass conservation. The mass conservation of the flow solver of the proposed numerical scheme has been already studied in [12]. There, for largely deforming impinging droplets without surfactants a mass loss of less than 1% has been observed. For investigating the mass conservation of the surfactant, we consider an unit sphere with the nonuniform surfactant distribution

$$\Gamma_0(\theta) = 0.5 + 0.5\cos\theta, \tag{16}$$

where θ is again the angular coordinate measured from the pole of the sphere. Instead of solving the Navier–Stokes equation for the fluid velocity, we move the free surface with the given prescribed divergence-free velocity

$$u = \left(\frac{x}{(x^2+y^2+z^2)^{3/2}}, \frac{y}{(x^2+y^2+z^2)^{3/2}}, \frac{z}{(x^2+y^2+z^2)^{3/2}}\right),$$

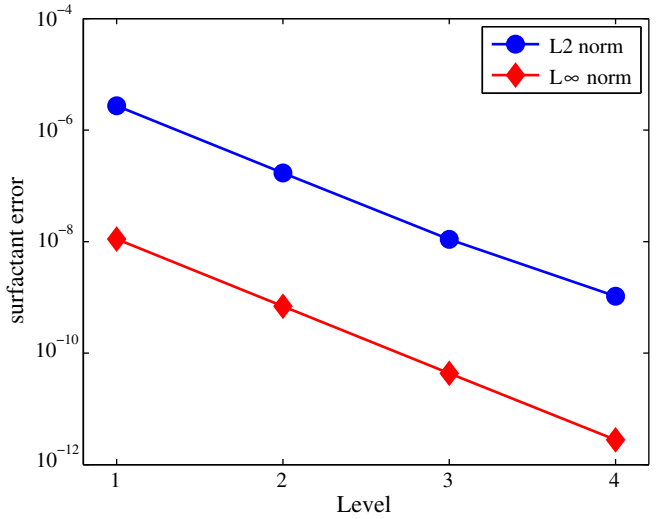

Fig. 1. Surfactant concentration error over the free surface of a fixed sphere.

normal to the free surface. The sphere starts to expand when time proceeds. Due to the free surface stretching, the surfactant concentration starts to decrease. Moreover, using $Pe = 10$ surfactant diffusion also takes place. When the mass of the surfactant is conserved, we should have

$$\int_{\Gamma_F(t)} \Gamma \, ds = 2\pi.$$

In the computation, we used the mesh of the diffusion test example and a time step of 10^{-5} on all mesh levels. The mass loss at the time $T = 0.25$ is shown in Fig. 2 for increasing mesh levels, and it is always below 1%. This shows the high accuracy of the proposed numerical scheme.

4.3. Marangoni convection

A convection driven by the variation of surface tension is called Marangoni convection. Since in flows with surfactants the surface tension becomes low when the surfactant concentration increases and vice verse, the presence of the surface tension gradient causes the liquid to move away from the low surface tension regime. In order to demonstrate this effect, we consider a spherical droplet in zero gravity space surrounded by a static ambient gas. Since the droplet is already in the equi-

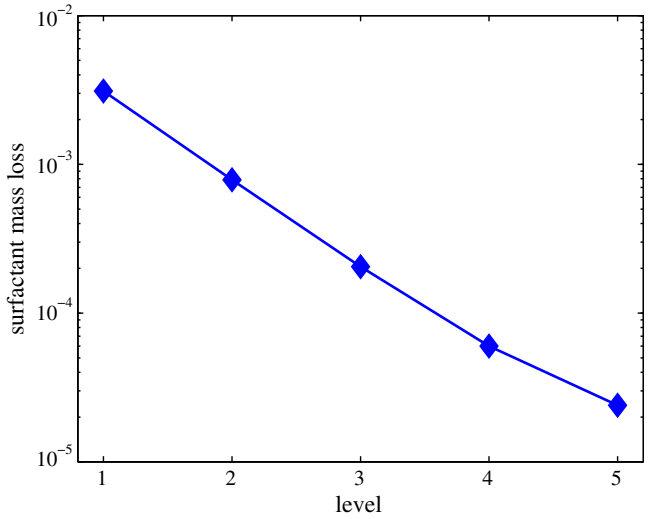

Fig. 2. The surfactant mass loss over the free surface of an expanding sphere.

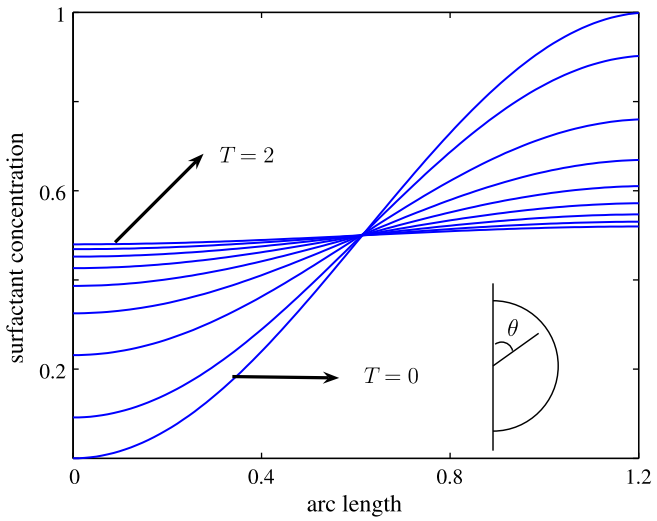

Fig. 3. Surfactant concentration profile over the free surface of a droplet at different instances for $Pe = 1$.

librium position, there will be no movement in the droplet if the surface force is also in equilibrium. However, this is not the case here, since we start with a nonuniform surfactant distribution over the droplet surface according to Eq. (16). Thus, the imbalances in the surface force induce a movement in the droplet. Note that this initial movement is entirely due to Marangoni convection.

In this test example, we have to solve both the Navier–Stokes equations and the surfactant concentration equation. First, we perform a computation for $Re = 1,\ We = 1$ and $Pe = 1$ until the time $T = 2$. The computationally obtained surfactant distributions over the arc length at different instance is presented in Fig. 3. Since the Peclet number in this computation is small, the surfactant distribution becomes almost uniform over a shot time $T = 2$. Next, to show the influence of the Peclet number, we perform an array of computations for the same test configuration with $Pe = 1$, 10, 100 and 1000. The surfactant distribution over the free surface at time $T = 2$ in each Peclet number case is presented in Fig. 4. The influence of the Peclet number is clearly visible. Further, also for a large Peclet number there is no oscillations in the numerical solution (even on a coarse mesh) as reported in the Volume-of-Fluid method [20]. This shows the advantage of using the boundary resolved mesh and the Lagrangian approach (no convection term) for solving the surfactant concentration equation.

4.4. Freely oscillation droplet

We consider a 3D-axisymmetric oscillating viscous liquid droplet surrounded by a static ambient gas. Initially, the droplet shape is perturbed from its equilibrium shape using

$$R(\theta) = R_0\left(1 + \epsilon S_k\left(\frac{\pi}{2} - \theta\right)\right),$$

where R is the distance from the center of the droplet to the free surface, R_0 is the radius of the spherical droplet, ϵ is a constant and k is the order of the spherical harmonic S_k. In all computations of oscillating droplet, we used $Re = 1000,\ We = 13.5,\ Pe = 10,\ k = 2$ and $\epsilon = 0.3$ with $L = R_0 = 1 \times 10^{-3}$ m and $U_{\text{ref}} = 1$ m/s.

4.4.1. Influence of mesh size

In this test case, we start at $t = 0$ with a uniform distribution of surfactant, i.e. $\Gamma(\theta, 0) = 0.5$. For the diffusion test on a fixed domain, in which an analytical solution is known, we studied the convergence order on a sequence of uniformly refined meshes. In the oscillating droplet case, we deal with highly unstructured moving meshes with a dynamically changing number of degrees of freedom (if remeshing is needed to guarantee a certain mesh quality). Under these circumstances, the usual approach to determine an experimental order of convergence by doing three computations on meshes of size $2h,\ h$ and $h/2$ cannot be applied. Nevertheless, we estimated the mesh quality by comparing the numerical results for three different meshes. For this we considered at time $t = 0$ three different initial meshes generated by the mesh generator Triangle [33] fixing 200, 600 and 800 degrees of freedom on the free surface. The resulting total numbers of degree of freedom have been 6674, 19,783 and 31,338. In the following, we refer to these variants as variant 1, 2 and 3, respectively. As shown in Fig. 5, the obtained trajectories of r_{max}, the maximal radius of the droplet in the radial direction, in all mesh variants are almost identical. However, small variations in the trajectory path are visible in the close-up view, see Fig. 6. We computed the frequency (ω_n) and the scaled damping factor (δ_n) after n periods given by

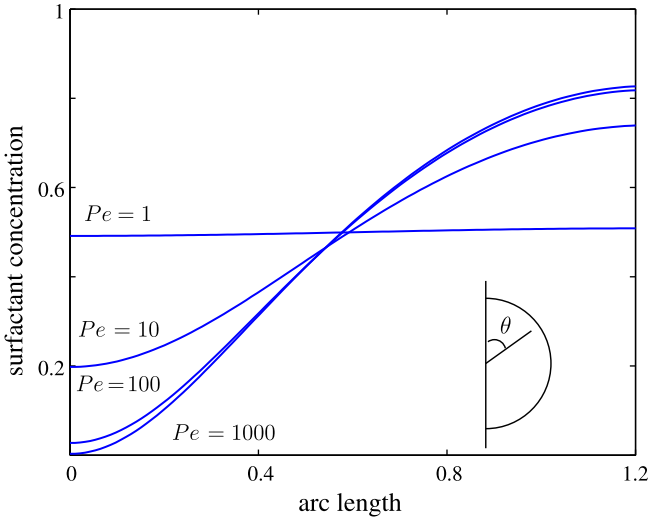

Fig. 4. Influence of the Peclet number on the surfactant concentration profile over the free surface of a droplet at time $T = 2$.

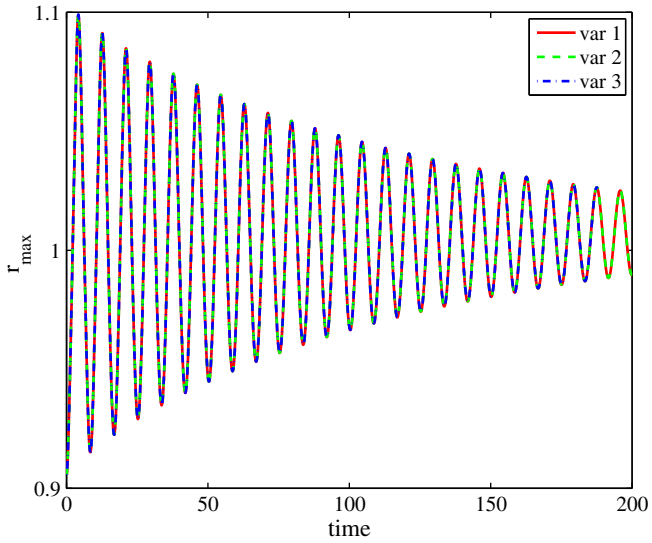

Fig. 5. The obtained trajectory of the r_{max} in a freely oscillating droplet in three variants of meshes with LEOS.

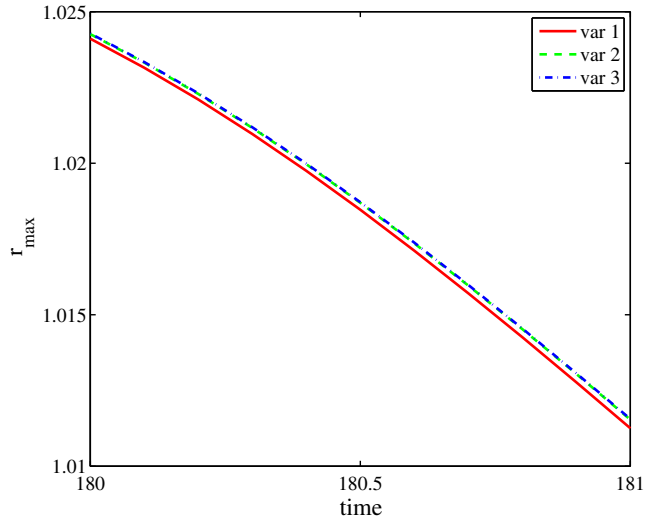

Fig. 6. The close-up view of the obtained trajectory of the r_{max} in a freely oscillating droplet in three variants of meshes with LEOS.

Table 1
Frequencies obtained after n periods on the coarsest mesh (var 1) with a uniform initial surfactant distribution and LEOS.

n	1	3	5	7	9	11	13	15
ω_n (1/s)	117.6	118.6	119	119.3	119.4	119.6	119.6	119.7

Table 2
The damping factor δ_n obtained in three different variants of meshes with a uniform initial surfactant distribution and LEOS.

n	1	3	5	7	9	11	13	15
var 1, δ_n	0.9161	0.9223	0.9257	0.9275	0.9287	0.9296	0.9301	0.9305
var 2, δ_n	0.9163	0.9223	0.9257	0.9275	0.9287	0.9295	0.9301	0.9305
var 3, δ_n	0.9163	0.9224	0.9257	0.9276	0.9287	0.9295	0.9301	0.9305

$$\omega_n = n/t_n, \quad \delta_n = \left(\frac{r_{max}(t_n) - r_\infty}{r(t_0) - r_\infty}\right)^{1/n},$$

where t_n is the time at the period n, and r_∞ is the radius of the spherical droplet with the same volume as the initial droplet and in our considered example $r_\infty = 1.00723$. In the numerically computed frequencies we saw no differences on the three meshes. Therefore, in Table 1 only the numbers computed on the coarsest mesh are given. Table 2 shows the small differences in the damping factor on the three different meshes. Further, a least squares fit of $(r_{max} - r_\infty)/(r(t_0) - r_\infty)$ to $(e^{-\lambda n + \mu_e})$ has been performed resulting in $\lambda = 0.07027$ and $\mu_e = 0.04293$ and which is in good agreement with the scaled damping

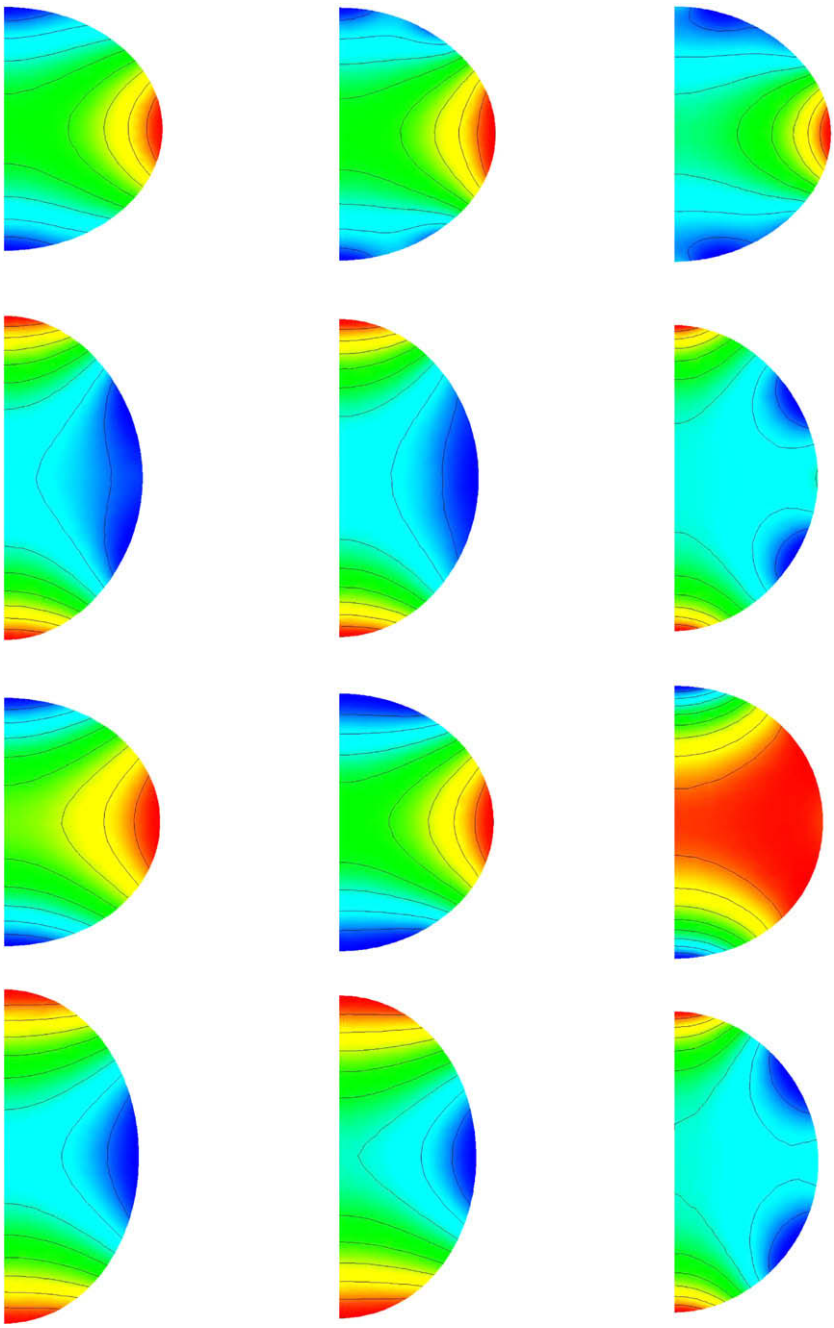

Fig. 7. A sequence of shapes and flow fields at different instances of a freely oscillating droplet, timings from top to bottom are $t = 4$, 7, 12 and 16. Colours represent the magnitude (red represents the maximum and blue represents the minimum in each image) of the pressure field in the droplet. (For interpretation of the references in color in this figure legend, the reader is referred to the web version of this article.)

factors. Moreover, the relative mass loss in each variant in the entire computation is less than 0.003% which underlines the high accuracy of the proposed numerical scheme.

4.4.2. Influence of surfactants

To study the influence of surfactants on the dynamic of the oscillating droplet, we consider the following three cases:

(i) surfactant-free (clean) free surface,
(ii) surfactant with linear equation of state (LEOS), and
(iii) surfactant with nonlinear equation of state (NLEOS).

For cases (ii) and (iii), initially, the surfactant is distributed nonuniformly over the free surface using

$$\Gamma(\theta, 0) = 0.9(1 - \sin\theta), \quad 0 \leqslant \theta \leqslant \pi.$$

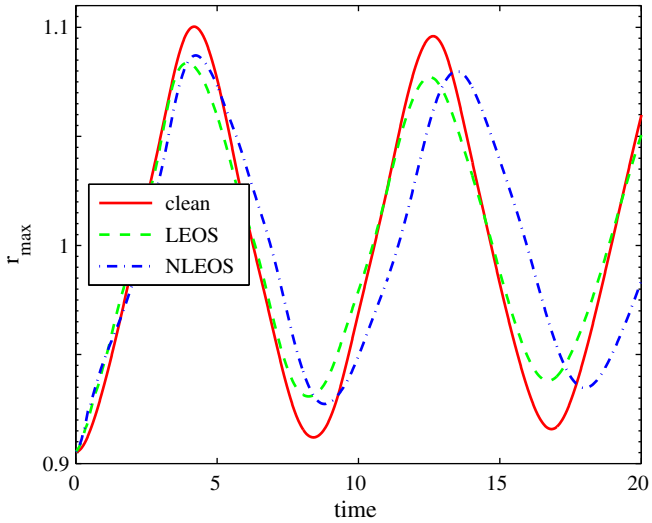

Fig. 8. The trajectory of the r_{max} in a freely oscillating droplet for (i) surfactant-free (clean) free surface, (ii) surfactant with linear equation of state (LEOS) and (iii) surfactant with nonlinear equation of state (NLEOS) cases.

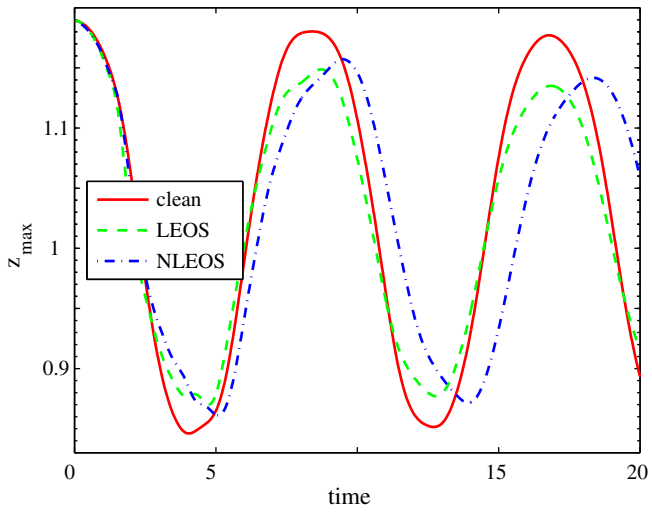

Fig. 9. The trajectory of the z_{max} in a freely oscillating droplet for (i) surfactant-free (clean) free surface, (ii) surfactant with linear equation of state (LEOS) and (iii) surfactant with nonlinear equation of state (NLEOS) cases.

Table 3
Numerically obtained frequencies ω_n for the freely oscillating droplet with a nonuniform initial surfactant distribution.

	ω_n (1/s)		
	Case (i)	Case (ii)	Case (iii)
$n = 1$	118.9	112.35	104.16
$n = 2$	119.91	119.04	108.69

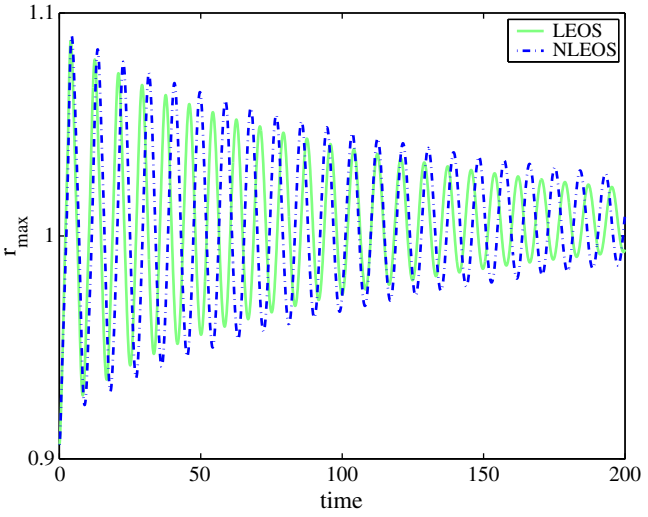

Fig. 10. The trajectory of the r_{max} in a freely oscillating droplet for the cases with the linear (LEOS) and nonlinear (NLEOS) equation of state.

Since the free surface is not in the equilibrium position, the droplet starts to oscillate around its equilibrium position even in the case (i) due to the imbalance of the surface force. In addition to that, in cases (ii) and (iii) a Marangoni convection takes place due to the nonuniform distribution of the surfactant. Computational results of the surfactant-free oscillating droplet (case i) with the considered flow parameters were already compared with the theoretical results in [14].

The obtained shapes and pressure isolines of the droplet at different instances are shown in Fig. 7 for the three cases. In each instance, the shape and the pressure distribution of the droplet for cases (i) and (ii) look similar. However, for the nonlinear equation of the state, case (iii), it looks different from cases (i) and (ii) at their respective instance. To see the surfactant effect, we calculated the trajectories of r_{max} and z_{max}, the maximal radius of the droplet in the radial and axial direction, respectively. Fig. 8 shows the trajectories of r_{max} for three different cases. Here, the difference between the clean and the surfactant contaminated cases can clearly be seen. In both LEOS and NLEOS cases, the amplitude is less in comparison with the clean surface case. A similar behaviour is also observed in Fig. 9, in which the trajectories of z_{max} for three different cases are presented. It is clear, since the presence of surfactants reduce the surface tension and eventually reduce the surface force, which is the main factor to induce the initial oscillations.

To show the effects of surfactant more clearly, we present the numerically obtained frequencies and the decay rate of oscillations for the considered cases. Table 3 shows the frequencies for all three cases which are calculated from the trajectory of z_{max} at $r = 0$ in their respective case. For the clean surface case (i), the numerically obtained frequency is in good agreement with the theoretically value 121.14 (see Ref. [14] for a comparison), which is obtained by the linear stability analysis for an inviscid oscillating droplet [4,22]. In the LEOS surfactant case (ii), the numerically obtained frequency after one period is less in comparison with the clean surface case (i) at the same period. During this initial period, the variation in the surfactant concentration is large and thus the influence of Marangoni forces will also be large. Since we considered a small Peclet number, the surfactant concentration becomes quickly almost uniform, say after $t = 5$, and hence the Marangoni effect becomes less pronounced at later stages. As a result, the frequency of the LEOS surfactant case (ii) becomes similar to the clean surface case (i), see Table 3 at $n = 2$. In contrast, the obtained frequency in the NLEOS surfactant case (iii) is much smaller even after the two periods.

Next, to study the difference in the LEOS and NLEOS more clearly, we run computations for cases (ii) and (iii) until time $T = 200$. The oscillations of the trajectory of r_{max} in both surfactant cases are shown in Fig. 10. Initially, the oscillations of the trajectory in the LEOS case (ii) are damped out more quickly than in the NLEOS case (iii). The computed frequencies of r_{max} after n periods in both cases are presented in Table 4. The frequency of the LEOS is similar as in the clean surface case (i). But, the frequency of the NLEOS case is smaller than the LEOS case which can also be seen in Fig. 10. The corresponding scaled

Table 4
Frequencies obtained in case (ii) (LEOS) and case (iii) (NLEOS) after n periods with a nonuniform initial surfactant distribution.

n	1	3	5	7	9	11	13	15
(ii) ω_n	119.05	119.05	119.33	119.66	119.84	119.96	120.04	120.10
(iii) ω_n	108.70	109.89	110.38	110.58	110.70	110.89	111.02	111.11

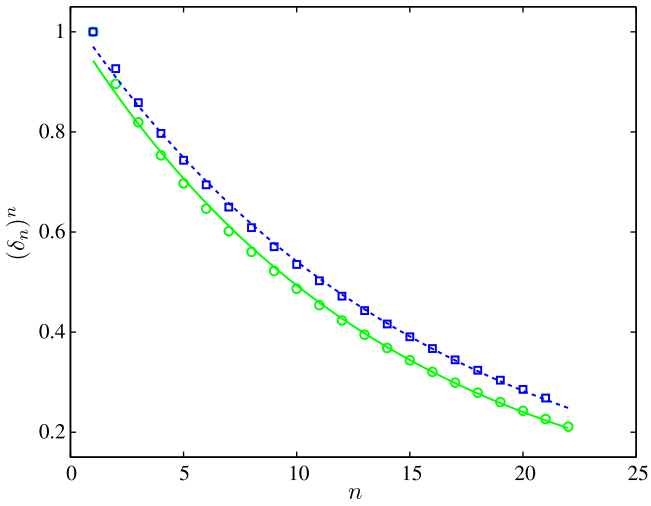

Fig. 11. The exponentially fitted $(e^{-\lambda n+\mu_e})$ scaled amplitude for the trajectories of r_{max} in Fig. 10. For curves with circle marker (LEOS) $\lambda = 0.07192,\ \mu_e = 0.01257$ and square marker (NLEOS) $\lambda = 0.06489,\ \mu_e = 0.03499$.

Table 5
The obtained damping factor δ_n for the decay rate of oscillations in case (ii) (LEOS) and case (iii) (NLEOS) at different periods n with a nonuniform initial surfactant distribution.

n	1	3	5	7	9	11	13	15
(ii) δ_n	0.8961	0.9098	0.9165	0.9206	0.9231	0.9248	0.9260	0.9270
(iii) δ_n	0.9265	0.9272	0.9296	0.9315	0.9329	0.9334	0.9348	0.9354

amplitude $(\delta_n)^n$ of the r_{max} trajectories in both cases over the period n are presented in Fig. 11. The decaying scaled amplitudes of LEOS and NLEOS cases are best fit with the exponential $(e^{-\lambda n+\mu_e})$ curve for $\lambda = 0.07192,\ \mu_e = 0.01257$ and $\lambda = 0.06489,\ \mu_e = 0.03499$, respectively. However, initially, there is a small difference between the scaled amplitude and their corresponding exponentially fitted curve in both cases. As we discussed in the above paragraph, this difference is due to the large variation in the initial surfactant distribution. A similar effect is observed in the damping factors for LEOS and NLEOS cases, see Table 5. Initially, the values of δ_n for LEOS case are small, and when the surfactant concentration becomes uniform, the values of δ_n for LEOS case become similar to the values in Table 2.

5. Summary

A moving mesh finite element scheme for computations of free surface flows with insoluble surfactants is presented in this paper. An arbitrary Lagrangian–Eulerian approach and the Lagrangian approach are used to solve the flow equations and the surfactant concentration equation, respectively. This allows for direct incorporation of both surface tension and Marangoni forces. Mathematical formulation to incorporate an arbitrary (either linear or nonlinear) equation of state, which relates the surface tension and the surfactants, into the numerical scheme is presented. Numerical results are compared with analytical solutions for a number of 3D-axisymmetric test problems to validate the numerical scheme. A convergence study on a uniformly refined fixed meshes has been made for the numerical scheme. Computational results for a freely oscillating 3D-axisymmetric droplet with and without surfactants are also presented. An excellent mass conservation for both the fluid and the surfactant is achieved in all test problems.

Acknowledgment

The authors would like to thank the DFG for supporting this research through the grant To143/9.

References

[1] D. Adalsteinsson, J.A. Sethian, Transport and diffusion of material quantities on propagating interfaces via level set methods, J. Comput. Phys. 185 (1) (2003) 271–288.
[2] M. Bertalmio, L.-T. Cheng, S. Osher, G. Sapiro, Variational problems and partial differential equations on implicit surfaces, J. Comput. Phys. 174 (2) (2001) 759–780.
[3] H.D. Ceniceros, The effects of surfactants on the formation and evolution of capillary waves, Phys. Fluid 15 (1) (2003) 245–256.
[4] S. Chandrasekhar, Hydrodynamics and Hydromagnetic Stability, Clarendon Press, Oxford, 1961.
[5] J. Donéa, Arbitrary Lagrangian–Eulerian finite element methods, in: T. Belytschko, T.R.J. Hughes (Eds.), Computational Methods for Transient Analysis, Elsevier Scientific Publishing Co., Amsterdam, 1983, pp. 473–516.
[6] G. Dziuk, Finite elements for the Beltrami operator on arbitrary surfaces, in: S. Hildebrandt, R. Leis (Eds.), Partial Differential Equations and Calculus of Variations, Springer, Berlin, 1988, pp. 142–155.
[7] G. Dziuk, An algorithm for evolutionary surfaces, Numer. Math. 58 (1991) 603–611.
[8] G. Dziuk, C.M. Elliott, Finite elements on evolving surfaces, IMA J. Numer. Anal. 27 (2007) 262–292.
[9] C.D. Eggleton, T.-M. Tsai, K.J. Stebe, Tip streaming from a drop in the presence of surfactants, Phys. Rev. Lett. 87 (2001) 048302.
[10] J. Fukai, Y. Shiiba, T. Yamamoto, O. Miyatake, D. Poulikakos, C.M. Megaridis, Z. Zhao, Wetting effects on the spreading of a liquid droplet colliding with a flat surface: experiment and modeling, Phys. Fluid 7 (2) (1995) 236–247.
[11] J. Fukai, Z. Zhao, D. Poulikakos, C.M. Megaridis, O. Miyatake, Modeling of the deformation of a liquid droplet impinging upon a flat surface, Phys. Fluid A 5 (11) (1993) 2588–2599.
[12] S. Ganesan, Finite element methods on moving meshes for free surface and interface flows, Ph.D. Thesis, Otto-von-Guericke-Universität, Fakultät für Mathematik, Magdeburg, published as book by docupoint Verlag Magdeburg, 2006. ISBN: 3-939665-06-1.
[13] S. Ganesan, L. Tobiska, Computations of flows with interfaces using arbitrary Lagrangian–Eulerian method, in: Proceedings of the ECCOMAS CFD 2006, Egmond aan Zee, The Netherlands. ISBN: 90-9020970-0.
[14] S. Ganesan, L. Tobiska, An accurate finite element scheme with moving meshes for computing 3D-axisymmetric interface flows, Int. J. Numer. Method Fluid 57 (2) (2008) 119–138.
[15] S. Ganesan, L. Tobiska, Modelling and simulation of moving contact line problems with wetting effects, Comput. Visual. Sci., in press. doi:10.1007/s00791-008-0111-3.
[16] D. Gerlach, G. Tomar, G. Biswas, F. Durst, Comparison of volume-of-fluid methods for surface tension-dominant two-phase flows, Int. J. Heat Mass Transfer 49 (3–4) (2006) 740–754.
[17] S. Gross, V. Reichelt, A. Reusken, A finite element based level set method for two-phase incompressible flows, Comput. Visual. Sci. 9 (4) (2006) 239–257.
[18] C. Hirt, B. Nichols, Volume of Fluid (VOF) method for the dynamics of free boundaries, J. Comput. Phys. 39 (1981) 201–225.
[19] C.W. Hirt, A.A. Amsden, J.L. Cook, An arbitrary Lagrangian–Eulerian computing method for all flow speeds, J. Comput. Phys. 14 (3) (1974) 227–253 (Reprinted in 135 (2) (1997) 203–216).
[20] A.J. James, J. Lowengrub, A surfactant-conserving volume-of-fluid method for interfacial flows with insoluble surfactant, J. Comput. Phys. 201 (2004) 685–722.
[21] V. John, G. Matthies, MooNMD – a program package based on mapped finite element methods, Comput. Visual. Sci. 6 (2–3) (2004) 163–170.
[22] H. Lamb, Hydrodynamics, Cambridge University Press, 1932.
[23] X. Li, C. Pozrikidis, The effect of surfactants on drop deformation and on the rheology of dilute emulsions in Stokes flow, J. Fluid Mech. 341 (1997) 165–194.
[24] P. Nithiarasu, An arbitrary Lagrangian–Eulerian (ALE) formulation for free surface flows using the characteristic-based split (CBS) scheme, Int. J. Numer. Method Fluid 12 (2005) 1415–1428.
[25] F. Nobile, Numerical approximation of fluid–structure interaction problems with application to haemodynamics, Ph.D. Thesis, École Polytechnique Fédérale de Lausanne, 2001.
[26] S. Osher, J.A. Sethian, Fronts propagating with curvature dependent speed: algorithms based on Hamilton–Jacobi formulations, J. Comput. Phys. 79 (1988) 12–49.
[27] J.E. Pilliod, E.G. Puckett, Second-order accurate volume-of-fluid algorithms for tracking material interfaces, J. Comput. Phys. 199 (2) (2004) 465–502.
[28] C. Pozrikidis, A finite-element method for interfacial surfactant transport, with application to the flow-induced deformation of a viscous drop, J. Eng. Math. 49 (2004) 163–180.
[29] M. Renardy, Y. Renardy, J. Li, Numerical simulation of moving contact line problems using a volume-of-fluid method, J. Comput. Phys. 171 (2001) 243–263.
[30] Y.Y. Renardy, M. Renardy, V. Cristini, A new volume-of-fluid formulation for surfactants and simulations of drop deformation under shear at a low viscosity ratio, Eur. J. Mech. B 21 (2002) 49–59.
[31] W. Rider, D. Kothe, Reconstructing volume tracking, J. Comput. Phys. 141 (1998) 112–152.
[32] J.A. Sethian, Level Set Methods, Cambridge University Press, 1996.
[33] J.R. Shewchuk, Triangle: engineering a 2D quality mesh generator and Delaunay triangulator, in: M.C. Lin, D. Manocha (Eds.), Applied Computational Geometry: Towards Geometric Engineering, Lecture Notes in Computer Science, vol. 1148, Springer-Verlag, 1996, pp. 203–222 (from the First ACM Workshop on Applied Computational Geometry).
[34] H.A. Stone, A simple derivation of the time-dependent convection–diffusion equation for surfactant transport along a deforming interface, Phys. Fluid A 2 (1) (1990) 111–112.
[35] M. Sussman, E.G. Puckett, A coupled level set and volume-of-fluid method for computing 3D axisymmetric incompressible two-phase flows, J. Comput. Phys. 162 (2000) 301–337.
[36] M. Sussman, P. Smereka, S. Osher, A level set approach for computing solutions to incompressible two-phase flow, J. Comput. Phys. 114 (1) (1994) 146–159.
[37] G. Tryggvason, B. Bunner, A. Esmaeeli, D. Juric, N. Al-Rawahi, W. Tauber, J. Han, S. Nas, Y.-J. Jan, A front-tracking method for the computations of multiphase flow, J. Comput. Phys. 169 (2) (2001) 708–759.
[38] S. Turek, Efficient Solvers for Incompressible Flow Problems. An Algorithmic and Computational Approach, Springer-Verlag, Berlin, 1999.
[39] S. Unverdi, G. Tryggvason, A front-tracking method for viscous, incompressible multi-fluid flows, J. Comput. Phys. 100 (1992) 25–37.
[40] M. van Sint Annaland, N. Deen, J. Kuipers, Numerical simulation of gas bubbles behaviour using a three-dimensional volume of fluid method, Chem. Eng. Sci. 60 (11) (2005) 2999–3011.
[41] H. Wong, D. Rumschitzki, C. Maldarelli, On the surfactant mass balance at a deforming fluid interface, Phys. Fluid 8 (1996) 3203–3204.
[42] J.-J. Xu, Z. Li, J. Lowengrub, H. Zhao, A level-set method for interfacial flows with surfactant, J. Comput. Phys. 212 (2006) 590–616.
[43] Y.W. Kruijt-Stegeman, F. van de Vosse, H. Meijer, Droplet behavior in the presence of insoluble surfactants, Phys. Fluid 16 (2004) 2785–2796.